NANO LETTERS

pubs.acs.org/NanoLett

Nonlinear Dark-Field Microscopy

Hayk Harutyunyan,[†] Stefano Palomba,[†] Jan Renger,[†] Romain Quidant,[†,§] and Lukas Novotny*[,†]

[†]Institute of Optics, University of Rochester, Rochester, New York 14627, United States, [†]ICFO-Institut de Ciencies Fotoniques, Mediterranean Technology Park, 08860 Castelldefels (Barcelona), Spain, and [§]ICREA-Institució Catalana de Recerca i Estudis Avançats, 08010 Barcelona, Spain

ABSTRACT Dark-field microscopy is a background-free imaging method that provides high sensitivity and a large signal-to-noise ratio. It finds application in nanoscale detection, biophysics and biosensing, particle tracking, single molecule spectroscopy, X-ray imaging, and failure analysis of materials. In dark-field microscopy, the unscattered light path is typically excluded from the angular range of signal detection. This restriction reduces the numerical aperture and affects the resolution. Here we introduce a nonlinear dark-field scheme that overcomes this restriction. Two laser beams of frequencies ω_1 and ω_2 are used to illuminate a sample surface and to generate a purely evanescent field at the four-wave mixing (4WM) frequency $\omega_{4wm} = 2\omega_1 - \omega_2$. The evanescent 4WM field scatters at sample features and generates radiation that is detected by standard far-field optics. This nonlinear dark-field scheme works with samples of any material and is compatible with applications ranging from biological imaging to failure analysis.

KEYWORDS Dark-field imaging, microscopy, nonlinear wave mixing, optical sensing, detection and failure analysis

The high sensitivity of dark-field microscopy has already been exploited in the 17th century by von Leeuwenhoek, Hooke, and Huygens.[1,2] A variant of dark-field miscroscopy, the ultramicroscope developed by Siedentopf and Zsigmondy in 1903, made it possible for the first time to observe single gold nanoparticles smaller than 10 nm in size.[3,4] Since then, many different variants of dark-field microscopy have been developed, including total internal reflection fluorescence microscopy (TIRF).[5,6] They all have in common that the detection of light scattered from a planar, featureless sample is suppressed, rendering a dark image. Light scattered or emitted from discrete sample features can therefore be detected against a "dark" background, which boosts the signal-to-noise ratio in the recorded images and allows very small sample features to be visualized. Background-free imaging and detection is the key ingredient in single molecule fluorescence studies[7,6] and in ultrasensitive detection.[8−11]

In dark-field microscopy, the excitation light path and its reflection from interfaces is excluded from the angular range of detection.[1,12] This restriction reduces the numerical aperture and affects the resolution. Here we introduce a nonlinear dark-field imaging scheme that does not restrict the angular detection range and allows dark-field imaging to be performed on any planar surface. Furthermore, it works for both transparent and opaque substrates in contrast to, for example, TIRF microscopy.

The principle of the imaging scheme is illustrated in Figure 1. Two laser beams of frequencies ω_1 and ω_2 irradiate a sample that is supported by a planar substrate. The laser beams are incident from angles θ_1 and θ_2 with respect to the surface normal and induce a third-order nonlinear polarization $\mathbf{P}$ in the substrate at the four-wave mixing (4WM) frequency $\omega_{4wm} = 2\omega_1 - \omega_2$.[13] The nonlinear polarization gives rise to a wave with frequency ω_{4wm} and propagation wavevector $\mathbf{k}_{4wm} = [k_{4wm,x}, 0, k_{4wm,z}]$ defined by momentum conservation.[13] For a substrate with a planar surface the condition for the in-plane component of $\mathbf{k}_{4wm}$ is

$$k_{4wm,x} = 2k_{1,x} - k_{2,x} = -2(\omega_1/c)n(\omega_1)\sin\theta_1 + (\omega_2/c)n(\omega_2)\sin\theta_2 \quad (1)$$

where c is the speed of light and n is the index of refraction of the medium from which the two exciting

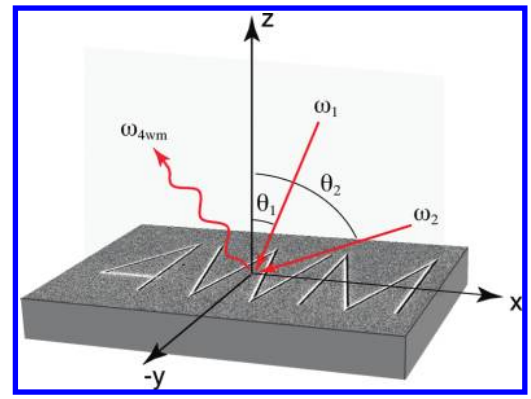

FIGURE 1. Illustration of the nonlinear dark-field imaging method. Two incident laser beams of frequencies ω_1 and ω_2 give rise to an evanescent four-wave mixing field at frequency $\omega_{4wm} = 2\omega_1 - \omega_2$. The evanescent field scatters at discrete sample features and gives rise to propagating radiation at ω_{4wm}.

* To whom correspondence should be addressed.
Received for review: 09/20/2010
Published on Web: 11/16/2010

DOI: 10.1021/nl1033304 | *Nano Lett.* **2010,** *10,* 5076–5079

fields are incident. The normal component of the 4WM wave follows from

$$k_{4\mathrm{wm},z} = \sqrt{n^2(\omega_{4\mathrm{wm}})\frac{\omega_{4\mathrm{wm}}^2}{c^2} - k_{4\mathrm{wm},x}^2} \qquad (2)$$

Evidently, for angles of incidence for which $k_{4\mathrm{wm},x} > n(\omega_{4\mathrm{wm}})\,\omega_{4\mathrm{wm}}/c$ the normal component of $\mathbf{k}_{4\mathrm{wm}}$ is imaginary and the 4WM wave is evanescent. Thus, there are angular ranges of θ_1 and θ_2 for which there is no 4WM radiation. For these angles, the 4WM field is confined to the very surface of the substrate and provides a means to excite the sample of interest nonradiatively.

The generated evanescent 4WM field can be converted into propagating radiation via scattering at discrete sample features. The scattered field can then be collected by an objective lens and focused on an image plane to render a dark-field image of the sample. Notice, that the excitation wavelength can be selected by adjusting the frequencies of the incident lasers. Furthermore, the spatial frequency $k_{4\mathrm{wm},x}$ of the 4WM excitation field can be tuned by the angles of incidence θ_1 and θ_2, and the polarization of the 4WM field can be selected by polarizers placed in the propagation paths of the incident lasers. The nonlinear dark-field imaging scheme works both in direct-projection mode, in which the entire sample is irradiated or in scanning-mode, where the incident lasers are focused to a spot and the sample is raster scanned. Scattering of surface bound 4WM fields at sample features renders information on the linear properties of the sample. On the other hand, for substrates of negligible nonlinearity, the dark-field scheme renders the nonlinear properties of the sample. Thus, by choosing suitable substrates the same setup can be used either for nonlinear dark-field imaging or for conventional nonlinear microscopy.

In our experiments, extinction spectra of sample features are obtained by recording the intensity of scattered 4WM radiation as a function of the wavelengths of the excitation lasers. The advantage of dark-field extinction spectroscopy is that no background is added to the scattered signal, which preserves the spectral lineshapes and facilitates the interpretation of recorded spectra. We use laser pulses of duration ~200 fs and ~76 MHz repetition rate and we choose incident wavelengths of $\lambda_1 = 800$ nm and $\lambda_2 = 1150$ nm to produce a four-wave mixing field in the visible at $\lambda_{4\mathrm{wm}} = 612$ nm. Average input powers are on the order of 1−5mW. Both laser beams are collimated to a beam of radius ~1 mm and then sent into an objective with numerical aperture of NA = 1.3 and back aperture of diameter 13 mm. The objective focuses the incident beams on the sample surface to spots with diameters of ~2 μm. The angles of incidence are determined by the relative distance of the incident beams from the optical axis in the back-focal plane of the objective.[14,15] The same objective is used to collect the scattered 4WM

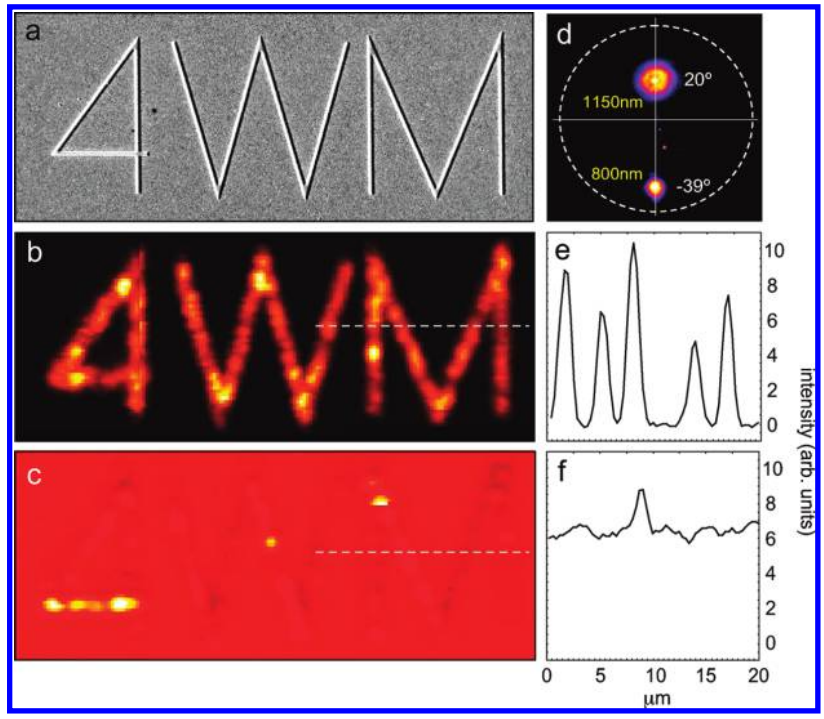

FIGURE 2. Images of a test sample consisting of letters 4WM made of TiO_2 and deposited on a gold surface. (a) SEM image, (b) nonlinear dark-field image recorded with $\theta_1 = -39°$ and $\theta_2 = 20°$, and (c) bright-field image recorded with $\theta_1 = \theta_2 = 20°$. (d) Image of the back focal plane of the focusing objective showing the positions of the excitation lasers for situation (b). (e,f) Cross sections along the lines indicated in (b) and (c), respectively.

DOI: 10.1021/nl1033304 | *Nano Lett.* **2010,** *10,* 5076–5079

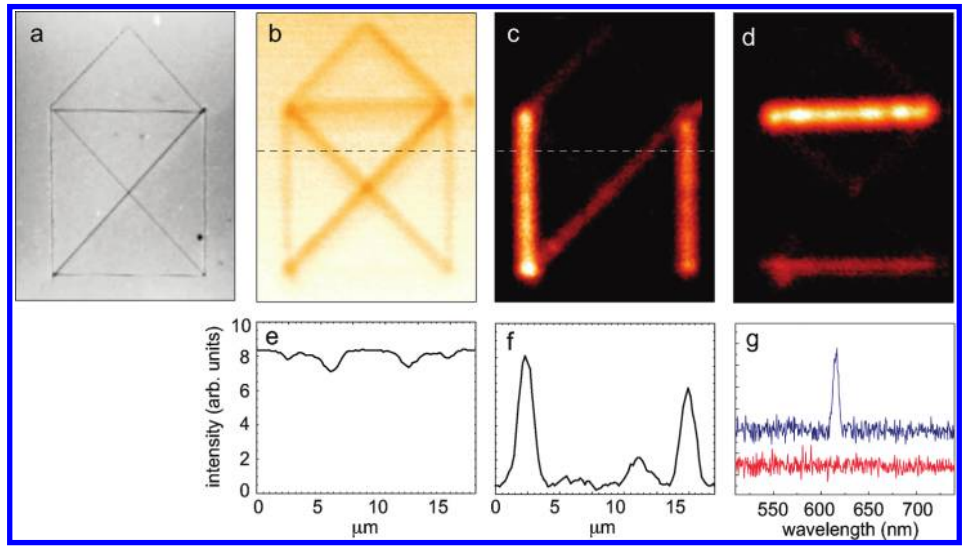

FIGURE 3. 4WM imaging of a silicon surface. The surface features a pattern that was scratched in with a diamond AFM tip. (a) AFM image showing scratches of depth 10−15 nm and width 180 nm. (b) Bright-field image recorded with $\theta_1 = \theta_2 = 20°$. (c) Dark-field image recorded with $\theta_1 = -39°$ and $\theta_2 = 20°$. The contrast in the dark-field image depends strongly on the plane of incidence of the excitation beams. Sample rotation allows different scratches to be highlighted. (d) Dark-field image with same parameters as in (c) but with the sample rotated by 90°. (e,f) Cross sections along the dashed lines in (b) and (c), respectively. (g) Spectrum of recorded radiation for excitation spot on (blue curve) and off (red curve) an individual scratch. For clarity, the spectra are vertically offset.

radiation and to either focus it on a photodetector or project it on a CCD camera.

To demonstrate the signal-to-noise gain of nonlinear dark-field imaging, we have fabricated test samples made of metallic and semiconducting substrates. The first test sample consists of the letters "4WM" made of TiO_2 and deposited on a gold substrate. The lines forming the letters have a height of 60 nm and width 200 nm. An electron micrograph of the test sample is shown Figure 2a and the corresponding nonlinear dark-field image recorded for incident angles $\theta_1 = -39°$ and $\theta_2 = 20°$ is rendered in panel b. The image is recorded by raster scanning the sample and detecting pixel-by-pixel the scattered 4WM radiation. The resolution can be significantly enhanced by using a pinhole in the detection path, or by exposing the entire sample surface at once and imaging the emitted 4WM radiation onto a CCD detector. However, in this report we are interested to demonstrate the high signal-to-noise ratio that can be achieved with the nonlinear dark-field imaging scheme. Clearly, to the side of the TiO_2 lines there is no measurable signal. The 4WM is only observed when the excitation spots coincide with the TiO_2 lines, which demonstrates that the nonlinear dark-field imaging scheme is essentially background-free. To compare the image contrast with a corresponding bright-field image, we move both excitation lasers to $\theta_1 = \theta_2 = 20°$. For these angles, the 4WM field is propagating and gives rise to a background at the detector. Figure 2c shows the resulting image of the same sample area. The letters can hardly be recognized and the signal-to-noise ratio is clearly worse, as evidenced by the line-cuts in panels e and f.

Similar results are obtained for other sample materials. In Figure 3, we show images of a test pattern scratched into a bare silicon surface. An atomic force microscope (AFM) with a diamond tip was used to create grooves of depth 10−15 nm and width 180 nm (Figure 3a). Again, the comparison between dark-field and bright-field imaging demonstrates that significantly higher contrast can be achieved in dark-field mode. Interestingly, we observe that the contrast in the dark-field image depends strongly on the plane of incidence of the excitation beams. In Figure 3c, the plane of incidence is horizontal, which yields a strong contrast for vertical scratches and a weak contrast for horizontal scratches. Rotating the sample by 90° renders the previously bright scratches dark and the dark scratches bright (Figure 3d). Evidently, this contrast is due to the polarization of the incident field and in the case of a highly anisotropic sample, the scattering cross-section can be varied by tuning the plane of incidence. Thus, in addition to a background-free contrast, the nonlinear 4WM imaging method also provides an orientation-selective contrast, which can be useful for identifying the nature of surface defects and contaminants.[16]

All the shown images have been recorded with *p* polarized excitation beams. The dependence on polarization angles is determined by the components of the third-order susceptibility tensor $\chi^{(3)}$ and hence by the crystal symmetry of the sample.[13] The spectrum of the emitted radiation, shown in Figure 3g, demonstrates that the 4WM line disappears if the excitation spots do not coincide with a scratch on the silicon surface, in agreement with the observed dark-field contrast in Figure 3c,d.

In conclusion, we have introduced a nonlinear dark-field imaging scheme, which does not restrict the angular detection range and which works with both transparent and opaque

DOI: 10.1021/nl1033304 | *Nano Lett.* **2010,** *10,* 5076–5079

samples. Furthermore, the scheme can be used to probe both the linear or nonlinear properties of the sample. The imaging scheme relies on nonlinear four-wave mixing, a third-order nonlinear process. At certain excitation angles, four-wave mixing generates fields that have momenta larger than propagating photons, which results in excitation of surface-bound evanescent waves. The efficiency of the imaging scheme depends on the $\chi^{(3)}$ tensor. Notice that the method is nonresonant and works for a variety of materials, including metals and semiconductors as demonstrated in this article. The recorded images feature interesting substructures (Figure 2b) and a contrast that depends on polarization and angle of incidence (Figure 3c,d). We believe that nonlinear dark-field imaging will find a broad range of interesting scientific and technological applications, ranging from biological imaging to failure analysis of materials and devices.

Acknowledgment. This work was supported by the National Science Foundation (Grant ECCS-0918416). We thank Brian McIntyre for the help in the preparation of the nanostructures.

REFERENCES AND NOTES

(1) Gage, S. H. *Trans. Am. Microsc. Soc.* **1920**, *39*, 95–141.
(2) Martin, L. V. *Microscopy* **1988**, *36*, 124–138.
(3) Siedentopf, H.; Zsigmondy, R. A. *Ann. Phys.* **1903**, *10*, 1–29.
(4) Sönnichsen, C.; Fritzsche, W. *100 years of Nanoscience with the Ultramicroscope*; Shaker Publishing: Herzogenrath, Germany, 2007.
(5) Axelrod, D.; Thompson, N.; Burghardt, T. *J. Microsc.* **1983**, *129*, 19–28.
(6) Mashanov, G. I.; Tacon, D.; Knight, A. E.; Peckham, M.; Molloyc, J. E. *Methods* **2003**, *29*, 142.
(7) Moerner, W. E.; Orrit, M. *Science* **1999**, *283*, 1670.
(8) Novo, C.; Funston, A. M.; Mulvaney, P. *Nat. Nanotechnol.* **2008**, *3*, 598–602.
(9) Liu, M.; Zentgraf, T.; Liu, Y.; Bartal, G.; Zhang, X. *Nat. Nanotechnol.* [Online early access]. doi:10.1038/nnano.2010.128.
(10) Sönnichsen, C.; Geier, S.; Hecker, N. E.; von Plessen, G.; Feldmann, J. *Appl. Phys. Lett.* **2000**, *77*, 2949–2951.
(11) Ignatovich, F. V.; Novotny, L. *Phys. Rev. Lett.* **2006**, *96*, No. 013901.
(12) Wayne, R. *Light and Video Microscopy*; Academic Press: Amsterdam, 2009.
(13) Renger, J.; Quidant, R.; Hulst, N. V.; Novotny, L. *Phys. Rev. Lett.* **2010**, *104*, No. 046803.
(14) Bouhelier, A.; Wiederrecht, G. P. *Opt. Lett.* **2005**, *30*, 884–886.
(15) Palomba, S.; Novotny, L. *Phys. Rev. Lett.* **2008**, *101*, No. 056802.
(16) Köklü, F. H.; Ippolito, S. B.; Goldberg, B. B.; Ünlü, M. S. *Opt. Lett.* **2009**, *34*, 1261.

DOI: 10.1021/nl1033304 | *Nano Lett.* **2010,** *10,* 5076–5079